Chemical Science

ROYAL SOCIETY OF CHEMISTRY

EDGE ARTICLE

View Article Online
View Journal | View Issue

Cite this: *Chem. Sci.*, 2024, **15**, 13290

All publication charges for this article have been paid for by the Royal Society of Chemistry

10-Dibenzothiophenyl-9,9-diphenylacridane-based multiple resonance emitters for high-efficiency narrowband green OLEDs with CIE $y > 0.7$ at high doping concentrations†

Rui Zhong,[ab] Mengyu Wang,[ab] Xingdong Wang,[a] Shumeng Wang,[a] Shiyang Shao*[ac] and Lixiang Wang *[ab]

Received 6th June 2024
Accepted 12th July 2024

DOI: 10.1039/d4sc03705g

rsc.li/chemical-science

Multiple resonance emitters are attractive for high-color-purity organic light-emitting diodes (OLEDs) because of their unique narrowband emissions; however, they are typically used at low doping concentrations (≤15 wt%) due to aggregation-caused quenching and spectral broadening induced by planar molecular skeletons. Here, we report two multiple resonance emitters (**BThPAc-1** and **BThPAc-2**) consisting of a 10-dibenzothiophenyl-9,9-diphenylacridane segment for efficient narrowband green emission at high doping concentrations. The dibenzothiophenyl-9,9-diphenylacridane segment contains two carbon-bridged phenyl rings as steric groups to inhibit intermolecular aggregation and a dibenzothiophene unit to extend conjugation and red-shift the emission to the green region. The resultant emitters exhibit narrowband emissions that peaked at 509–510 nm with a full width at half-maximum (FWHM) of 32 nm in 1 wt% doping films, which are maintained at less than 35 nm even in neat films. Remarkably, OLEDs employing the emitters reveal pure-green electroluminescence with a maximum external quantum efficiency of 20.3% and CIE coordinates of (0.18, 0.72) at 30 wt% doping concentration, which represents the best color coordinates for green multiple resonance OLEDs at high doping concentrations.

1 Introduction

Thermally activated delayed fluorescence (TADF) emitters are attractive for organic light-emitting diodes because of their capability to utilize triplet excitons by the reverse intersystem crossing (RISC) process without the use of noble metals. To realize the rapid RISC process, a small energy gap (ΔE_{ST}) between singlet (S_1) and triplet (T_1) states is required for TADF emitters.[1–4] In this regard, TADF emitters are generally designed based on twisted donor–acceptor (D–A) architecture to minimize the overlap between the highest occupied molecular orbital (HOMO) and lowest unoccupied molecular orbital (LUMO) to reduce ΔE_{ST}.[5–7] However, such D–A type TADF emitters are accompanied by strong intramolecular charge transfer (ICT) character with large structural relaxation in excited states, leading to a large Stokes shift and a broad emission spectrum with full width at half-maximum (FWHM) larger than 70 nm, unfavourable for application in high-resolution displays requiring pure red/green/blue (R/G/B) emissions.[8–10]

Recently, multiple resonance thermally activated delayed fluorescence (MR-TADF) emitters have attracted much attention of researchers because of their narrowband emissions that can overcome the drawbacks of broad emission bands for D–A type TADF emitters.[11–15] In general, MR-TADF emitters are composed of polycyclic aromatic hydrocarbon (PAH) skeletons embedded with electron-rich atoms (nitrogen, oxygen, sulfur, and selenium) and electron-deficient atoms/groups (boron/carbonyl) with opposite electronic effects.[16–27] This arrangement of heteroatoms induces the atomic separation of the HOMO and LUMO with non-bonding orbitals, resulting in reduced vibration relaxation and narrowband emissions with FWHM less than 40 nm.[28–33] By rational design of molecular structures, full-color MR-TADF emitters with emission covering the whole visible light range and EQE > 30% have been developed.[34–39] Despite this progress, MR emitters still suffer from severe aggregation-caused quenching (ACQ) and spectral broadening

[a]State Key Laboratory of Polymer Physics and Chemistry, Changchun Institute of Applied Chemistry, Chinese Academy of Sciences, Changchun, Jilin 130022, China. E-mail: lixiang@ciac.ac.cn

[b]School of Applied Chemistry and Engineering, University of Science and Technology of China, Hefei, Anhui 230026, China

[c]State Key Laboratory of Marine Resource Utilization in South China Sea, School of Materials Science and Engineering, Hainan University, Haikou, Hainan 570228, China. E-mail: ssyang@hainanu.edu.cn

† Electronic supplementary information (ESI) available. CCDC 2350022. For ESI and crystallographic data in CIF or other electronic format see DOI: https://doi.org/10.1039/d4sc03705g

at high doping concentrations due to their planar structure and strong intermolecular aggregation, making them always used at relatively low-concentration doped films (≤15 wt%).[40–51] Although much attention has been paid to the introduction of bulky groups into MR-TADF for providing steric hindrance to reduce intermolecular interaction,[52–63] it is still challenging to develop MR emitters with green emission (CIE y value > 0.70) that are insensitive to doping concentrations.[64–69] For instance, 5,11-diphenyl-5,11-dihydroindolo[3,2-*b*]carbazole (ICz)-based emitters (BN-ICz-1 and BN-ICz-2)[50] have been reported to exhibit reduced vibration and a small FWHM of 21 nm, giving green emission at 522 nm with CIE coordinates of (0.24, 0.73) in OLED devices. Nevertheless, these emitters worked at low doping concentrations of 1–5 wt%. Similarly, MR emitters with the nitrogen atom fused at different positions[49] (BN-TP-N4) have been reported to show high-color-purity green emission with a CIE y value of 0.70 at 3 wt% doping concentration but deteriorating to CIE y < 0.70 at 5 wt% concentration. Actually, green MR emitters with CIE y > 0.70 at high doping concentrations (>15 wt%) are not reported in the literature so far.

Here, we report two green MR-TADF emitters (**BThPAc-1** and **BThPAc-2**) consisting of a 10-dibenzothiophenyl-9,9-diphenylacridane-based B, N-doped polycyclic skeleton for efficient narrowband OLEDs with high color-purity even at high doping concentration (Fig. 1). This molecular design utilizes two carbon-bridged phenyl rings of a dibenzothiophenyl-9,9-diphenylacridane segment as to provide steric hindrance to suppress aggregation of the polycyclic skeleton, and a dibenzothiophene unit to extend conjugation and red-shift the emission to the green region. As a result, the emitters **BThPAc-1** and **BThPAc-2** exhibit green emissions at 509–510 nm with a narrow FWHM of 32 nm at 1 wt% doping concentration, which are maintained at 515–520 nm with FWHM of 34–35 nm even in neat films. OLED devices based on the emitters exhibit green electroluminescence with an emission peak at 514 nm, FWHM of 33 nm, CIE coordinates of (0.16, 0.71) and a maximum EQE of 26.5% at a low doping concentration of 3 wt%. Remarkably, at a high doping concentration of 30 wt%, the OLEDs still maintain the high color purity with CIE coordinates of (0.18, 0.72) for a maximum EQE of 20.3%, representing the best color coordinates for green MR-TADF OLEDs at high doping concentrations (>15 wt%, Table S7†).

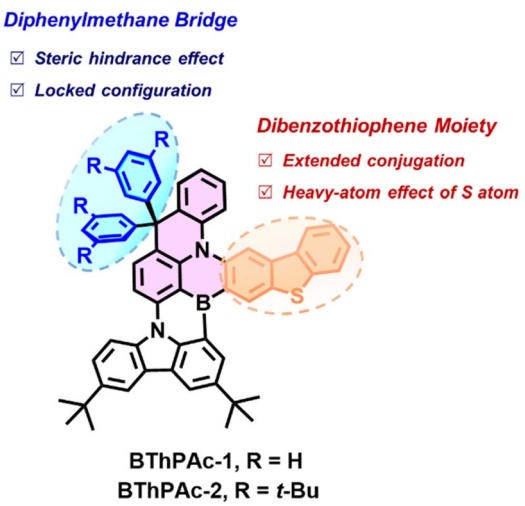

Fig. 1 Molecular design of multiple resonance emitters BThPAc-1 and BThPAc-2.

2 Results and discussion

The synthesis of **BThPAc-1** and **BThPAc-2** is outlined in Scheme 1. 1-Bromo-2-chloro-3-fluorobenzene was used as a starting material which underwent nucleophilic substitution with 3,6-bis(*tert*-butyl)-carbazole and the Buchwald coupling reaction with methyl 2-aminobenzoate to afford the ester intermediate **2**. Subsequently, **2** was reacted with phenylmagnesium bromide or 3,5-di-*tert*-butylphenylmagnesium bromide and then with boron trifluoride etherate to form the key acridan intermediates **3a** and **3b**, followed by coupling with 2-bromodibenzothiophene to afford the chloride precursors **4a** and **4b**. The precursors were lithiated and underwent intramolecular electrophilic borylation with boron tribromide and *N*,*N*-diisopropylethylamine to give the desired products **BThPAc-1** and **BThPAc-2** in yields of 40–60%. To investigate the role of the fused thiophene moiety, the MR emitter without the dibenzothiophene moiety (**PAc**) was also synthesized from **3a** through the same synthetic procedure except by using bromobenzene instead of 2-bromodibenzothiophene to form the chloride precursor. The synthesized compounds were identified by ^{1}H and ^{13}C NMR spectra and mass spectra (Fig. S13–S34†). Thermogravimetric analysis shows that both **BThPAc-1** and **BThPAc-2** exhibit good thermal stability with decomposition temperatures (5% weight) above 400 °C, suitable for the preparation of OLED devices by the vacuum evaporation process. The electrochemical properties of **BThPAc-1** and **BThPAc-2** were characterized by cyclic voltammetry, which show reversible oxidation waves with onset potentials (E^{ox}_{onset}) at 0.55 and 0.49 V, and irreversible reduction waves with onset potentials (E^{red}_{onset}) at −1.98 and −1.99 V, respectively. According to the oxidation and reduction onset potentials, HOMO/LUMO levels were determined to be −5.35/−1.98 eV and −5.29/−2.02 eV for **BThPAc-1** and **BThPAc-2**, respectively.

To investigate the crystallographic structure of the emitters, single crystals are grown by slowly evaporating the solvent of a solution of the samples in a dichloromethane/*n*-hexane mixture (1/2, v/v) at 20 °C to form needle-like crystals of **BThPAc-1** that can be characterized by synchrotron radiation X-ray diffraction. As shown in Fig. 2, the geometry of **BThPAc-1** exhibits a quasi-planar configuration for the polycyclic skeleton with typical B–C, N–C and S–C bond lengths of 1.535–1.536 Å, 1.395–1.431 Å and 1.739–1.754 Å, respectively. Remarkably, the two carbon-bridged phenyl groups are almost perpendicular to the polycyclic skeleton plane, providing steric hindrance for the central MR skeleton. In the packing model, a strong steric effect of the perpendicular phenyl groups forces two adjacent **BThPAc-1** molecules to stack in a head-to-head and tail-to-tail pattern. Two types of π···π interactions are observed which belong to two carbazole groups with a distance of 3.554 Å and two

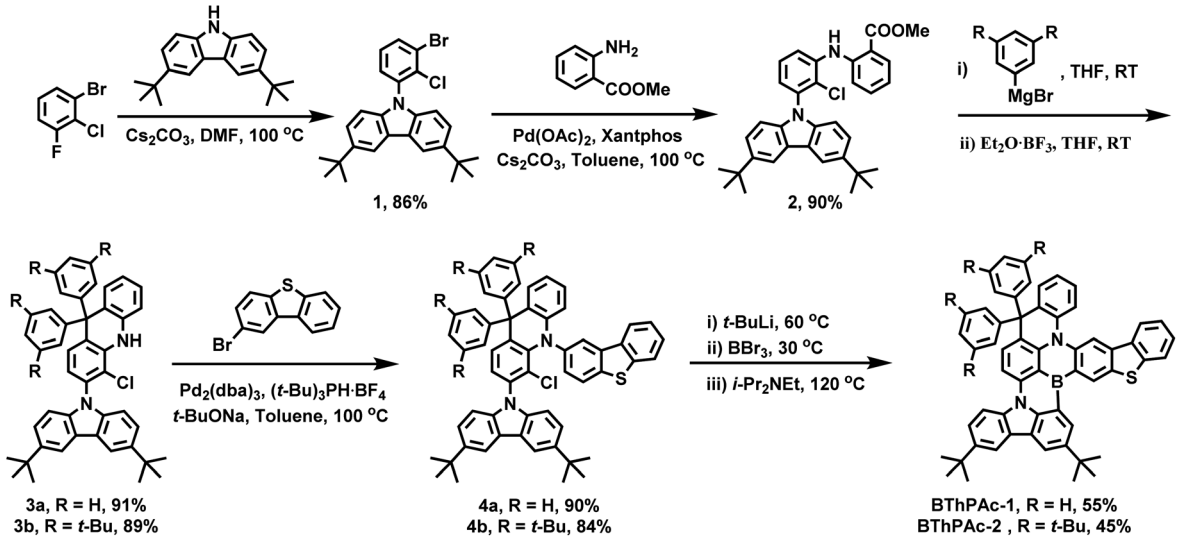

Scheme 1 Synthetic routes for **BThPAc-1** and **BThPAc-2**.

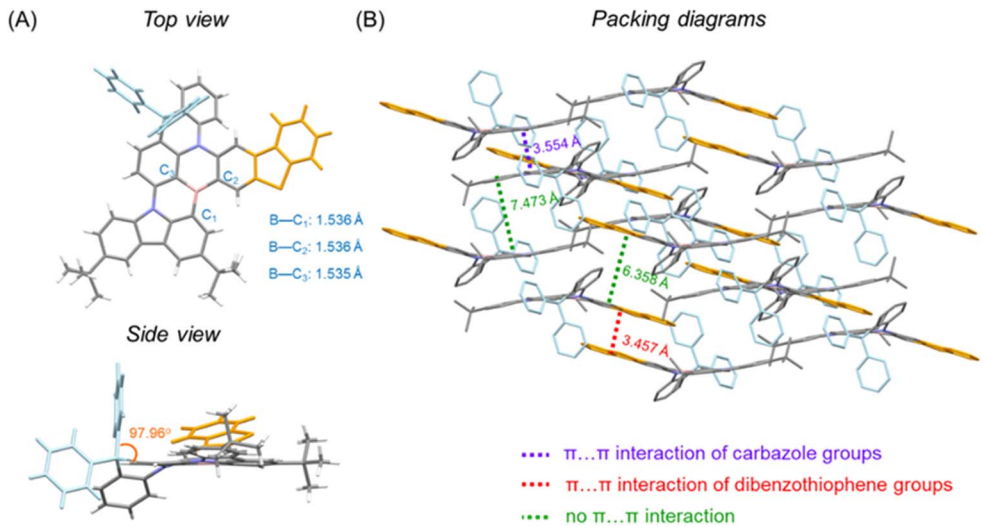

Fig. 2 (A) Single-crystal structure and (B) packing diagrams for **BThPAc-1**.

dibenzothiophene groups with a distance of 3.457 Å, respectively, corresponding to quasi-dimers. However, other π-groups are staggered due to steric hindrance of the carbon-bridged phenyl rings, leading to enlarged distances over 6.0 Å and effectively suppressed intermolecular interactions.

To gain insight into photophysical properties of two emitters, density functional theory (DFT) and time-dependent DFT (TD-DFT) calculations are carried out at the M062x/def2-SVP level to calculate their optimized ground and excited state geometries and frontier molecular orbital (FMO) distributions. To accurately determine excited state energy levels for the emitters, a second-order approximate coupled-cluster with singles and doubles (SCS-CC2) model is also employed using the cc-pVDZ basis set.[70] As depicted in Fig. 3 and S1–S4,† HOMOs are mainly localized on nitrogen atoms and their *ortho*-/*para*-positions of the surrounding phenyl rings, while LUMOs are localized on boron atoms and their *ortho*-/*para*-positions, corresponding to atomically separated FMO distributions for typical MR emitters. Notably, compared to **PAc** without the dibenzothiophenyl moiety, **BThPAc-1** and **BThPAc-2** exhibit extended HOMO and LUMO distributions to peripheral dibenzothiophenyl moieties, indicating larger conjugation of the polycyclic skeleton. Consequently, S_1 energy levels of **BThPAc-1** and **BThPAc-2** (2.91–2.94 eV) are lower than that of **PAc** (3.08 eV). The ΔE_{ST} values for **BThPAc-1** and **BThPAc-2** are 0.11–0.12 eV, which are small enough to promote the RISC process. Meanwhile, the emitters exhibit a small root mean square deviation (RMSD) of 0.09 and a small reorganization energy of 0.14–0.16 eV between S_0 and S_1 states, indicating a small structural change upon excitation. It is noted that **BThPAc-1** and **BThPAc-2** have considerable SOC matrix elements (SOCME) between singlet states (S_n) and triplet states

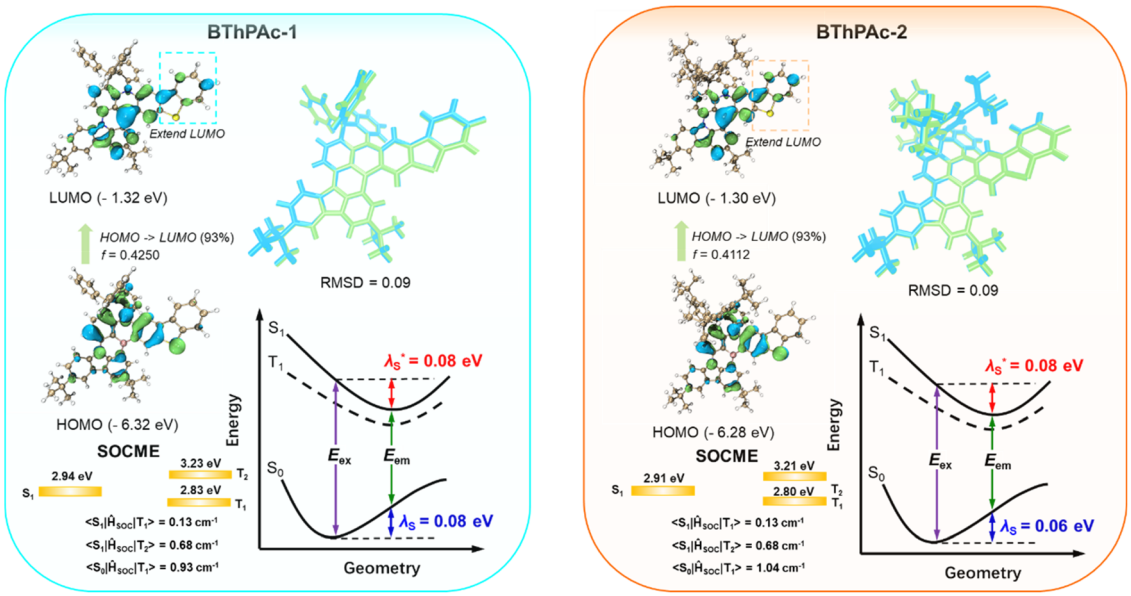

Fig. 3 HOMO/LUMO distributions, SOCME and reorganization energy for **BThPAc-1** and **BThPAc-2**.

(T_n) (0.13–0.68 for S_1–T_n ($n = 1$–2) and 0.91–1.04 for S_0–T_1). Such SOC matrix element values are much larger than those of **PAc** without the dibenzothiophenyl moiety (0.13–0.14 for S_1–T_n ($n =$ 1–2) and 0.73 for S_0–T_1), indicating that the sulfur atom in the dibenzothiophenyl moiety can play a crucial role in enhancing spin–orbital coupling.

To investigate photophysical properties, UV-vis absorption and photoluminescence spectra of **BThPAc-1** and **BThPAc-2** in dilute toluene solution (10^{-5} M) were measured. As shown in Fig. 4(A) and (B), **BThPAc-1** and **BThPAc-2** show two absorption bands at 404–405 nm and 485–488 nm in toluene, which are assigned to π–π* transitions of polycyclic skeletons and intramolecular charge-transfer (ICT) transitions, respectively (Table 1). While for PL spectra, **BThPAc-1** and **BThPAc-2** exhibit intense and sharp emissions at 508 and 509 nm in toluene, respectively, corresponding to a small Stokes shift of 21–23 nm typical for the multi-resonance emitters. Compared to **PAc** with an emission maximum of 484 nm, the emission peaks for **BThPAc-1** and **BThPAc-2** are red-shifted by 24–25 nm, consistent with their extended conjugation and reduced S_1 energy level, as predicted by TD-DFT calculations. It is noted that the FWHM values for **BThPAc-1** and **BThPAc-2** (∼30 nm) are the same as that of **PAc**, indicating that extension of conjugation barely affects the narrowband emission characteristics for the MR skeleton. PL spectra of the emitters in solvents with different polarities show a slight red-shift and broadening as the solvent polarity increases, consistent with their short-range ICT characteristic. According to onsets of fluorescence and phosphorescence spectra at 77 K, the experimental S_1/T_1 state energy levels are 2.57/2.41 eV and 2.55/2.40 eV for **BThPAc-1** and **BThPAc-2**, respectively, giving small ΔE_{ST} values of 0.15–0.16 eV. The PLQY for the emitters measured in doped films (5 wt% doping ratios in mCP) are 88–89%, which are higher than that of **PAc** (PLQY = 83%). To demonstrate the effect of bridged phenyl rings on aggregation behaviors in the solid state, the dependence of PL spectra of the emitters on the doping concentration is investigated. As shown in Fig. 4(E) and (F), **BThPAc-1** exhibits narrowband green emission at 509 nm with an FWHM of 32 nm at a low concentration of 1 wt%. As the doping concentration gradually increases to 100 wt%, the emission band is red-shifted by 11 nm (from 509 to 520 nm), while the FWHM is slightly increased to 35 nm. For **BThPAc-2** containing *tert*-butyl groups in two phenyl units, the red shift of emission is decreased by 5 nm (from 510 to 515 nm), and the FWHM value is broadened by only 2 nm (from 32 to 34 nm). These results indicate that intermolecular interaction and aggregation-caused spectral broadening can be efficiently suppressed by incorporating two carbon-bridged phenyl units into the MR skeleton.

Transient PL decay spectra of **BThPAc-1** and **BThPAc-2** are shown in Fig. 4(C) and (D), which reveal both prompt fluorescence with lifetimes of 7.0–7.1 ns and delayed fluorescence with lifetimes in the range of 12.7–13.0 μs. As the temperature increases from 200 K to 300 K, the delayed components of two emitters increase corresponding to the thermally activated triplet-to-singlet up-conversion process. The ratios of delayed components are 30% and 32% for **BThPAc-1** and **BThPAc-2**, respectively, giving rate constants of prompt fluorescence (k_r), intersystem crossing (k_{ISC}) and k_{RISC} of 0.9–1.0 × 10^8, 4.2–4.3 × 10^7 and 1.1–1.2 × 10^5 for **BThPAc-1** and **BThPAc-2**, respectively. Notably, k_{ISC} and k_{RISC} for **BThPAc-1** and **BThPAc-2** are much larger than those of **PAc** ($k_{ISC} = 1.5 \times 10^7$ and $k_{RISC} = 0.6 \times 10^5$), indicating that intersystem crossing between singlet and triplet states can be accelerated by the enhanced SOC.

To investigate electroluminescence properties of the two emitters, OLEDs with the configuration of indium tin oxide (ITO)/(1,1-bis[(di-4-tolylamino)phenyl]cyclohexane) (TAPC) (90 nm)/(tris(4-carbazolyl-9-ylphenyl)amine) (TCTA) (5 nm)/3,3′-

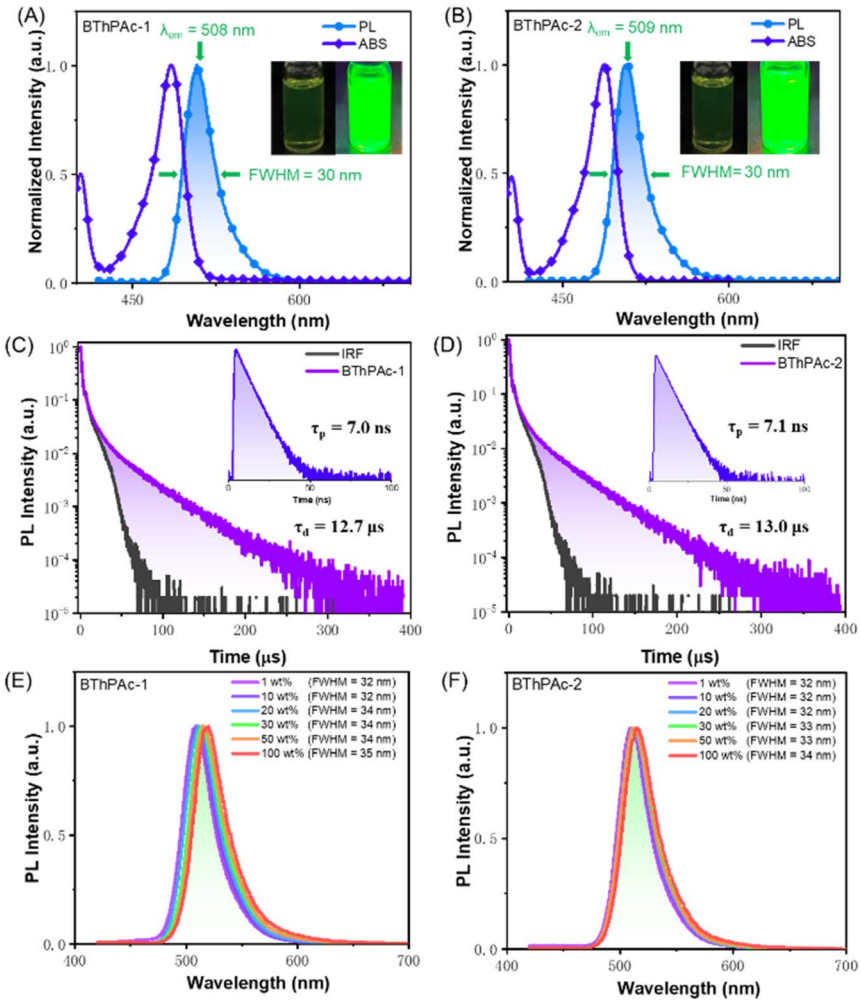

Fig. 4 (A and B) UV-visible absorption and PL spectra of **BThPAc-1** and **BThPAc-2** in toluene with a concentration of 10^{-5} M. (C and D) Transient PL decay curves for **BThPAc-1** and **BThPAc-2** doped films in 1 wt% mCP. (E and F) PL spectra of **BThPAc-1** and **BThPAc-2** doped films in mCP with different dopant concentrations.

Table 1 Summary of photophysical properties of **BThPAc-1** and **BThPAc-2**

	λ_{abs}[a] [nm]	λ_{em}[b] [nm]	FWHM[c] [nm]	Φ_{PLQY}[d]	τ_p/τ_d[e] [ns μs^{-1}]	k_r[f] [10^7 S^{-1}]	k_{ISC}[f] [10^7 S^{-1}]	k_{RISC}[f] [10^5 S^{-1}]	S_1/T_1[g] [eV]	ΔE_{ST}[h] [eV]
BThPAc-1	485	508	30	0.88	7.0/12.7	9.0	4.3	1.1	2.57/2.41	0.16
BThPAc-2	488	509	30	0.89	7.1/13.0	9.0	4.2	1.2	2.55/2.40	0.15

[a] Absorption peak measured in toluene solution (10^{-5} M). [b] Emission peak measured in toluene solution (10^{-5} M). [c] Full width at half maximum of the PL spectrum. [d] Photoluminescence quantum yield measured in doping films in mCP (5 wt%). [e] Prompt and delayed fluorescence lifetimes of doping films. [f] k_r, k_{ISC} and k_{RISC} represent the rate constants of radiative decay of S_1, intersystem crossing from S_1 to T_1 and reverse intersystem crossing from T_1 to S_1. [g] Singlet (S_1) and triplet (T_1) state energy levels estimated from fluorescence and phosphorescence spectra. [h] Energy gap between S_1 and T_1.

bis(*N*-carbazolyl)-1,1′-biphenyl (mCBP) (5 nm)/2-(5-(4,6-diphenyl-1,3,5-triazin-2-yl)-2-methylphenyl)-1-phenyl-benzo[*d*] imidazole (BIZ-6Me-TRZ): 1–30 wt% emitter (30 nm)/(5-tri(m-pyrid-3-yl-phenyl)benzene) (TmPyPB) (45 nm)/LiF (1 nm)/Al (150 nm) were fabricated. The chemical structure and energy diagram of materials used for OLED devices are illustrated in Fig. 5(A) and (B), and the device performance is displayed in Fig. 5(C)–(E). As shown in Fig. 5(D), devices using 1 wt% **BThPAc-1** and **BThPAc-2** as emitters exhibit emission peaks at 512 and 511 nm, accompanied by FWHM of 34 and 33 nm, respectively, corresponding to Commission International de l'Eclairage (CIE) coordinates of (0.15, 0.70) and (0.14, 0.69) (Table 2). As the emitter concentration increases from 1 to 30 wt%, the emission peak shifts slightly from 511–512 nm to

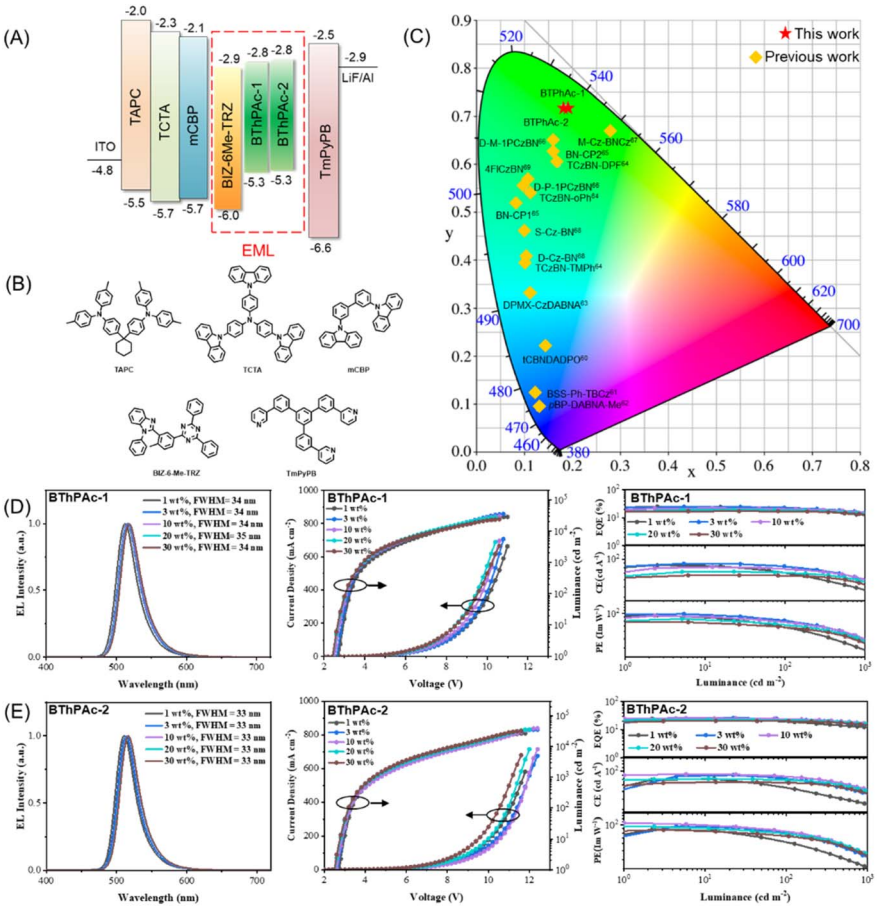

Fig. 5 (A) Device configuration for **BThPAc-1** and **BThPAc-2**. (B) Chemical structures of materials used for the devices. (C) CIE coordinates for **BThPAc-1**, **BThPAc-2** and reported aggregation-resistant MR-TADF emitters at high doping concentrations (>15 wt%) (Table S7†). (D and E) OLED device performance for **BThPAc-1** and **BThPAc-2**.

517–518 nm, and the FWHMs are maintained at 33–34 nm, giving CIE coordinates of (0.19, 0.72) and (0.18, 0.72) for **BThPAc-1** and **BThPAc-2**, respectively, which are the best color coordinates for green MR-TADF OLEDs at high doping concentrations (>15 wt%) (Table S7†).

The current density (*J*)–voltage (*V*)–luminance (*L*) and EQE–*L*–luminous efficiency (LE) characteristics of the OLEDs are shown in Fig. 5(D) and (E). The devices show low turn-on voltages (at a luminance of 1 cd m^{-2}) of 2.4–2.7 V for **BThPAc-1** and **BThPAc-2**. From the EQE–*L* characteristics of devices, it can be

Table 2 Summary of OLED device performance for **BThPAc-1** and **BThPAc-2**

	Doping concentration	V_{on}[a] [V]	L_{max}[b] [cd m^{-2}]	CE_{max}[c] [cd A^{-1}]	PE_{max}[d] [lm W^{-1}]	$EQE_{Max/100/1000}$[e] [%]	FWHM[f] [nm]	λ_{EL}[g] [nm]	CIE[h] (*x*, *y*)
BThPAc-1	1 wt%	2.67	28 560	84.2	94.5	25.2/20.6/12.4	33.9	512	0.152, 0.702
	3 wt%	2.61	35 443	87.9	98.7	24.8/22.8/15.5	34.3	516	0.171, 0.718
	10 wt%	2.47	30 277	79.6	93.1	22.0/20.9/15.2	34.5	517	0.181, 0.721
	20 wt%	2.41	27 497	69.5	83.6	19.0/18.5/14.0	34.7	518	0.187, 0.721
	30 wt%	2.41	23 844	62.7	75.5	17.0/16.9/12.9	34.4	518	0.191, 0.720
BThPAc-2	1 wt%	2.68	26 918	79.9	86.9	24.7/19.6/12.1	32.7	511	0.143, 0.693
	3 wt%	2.64	35 737	89.9	100.9	26.5/22.0/14.4	32.7	514	0.157, 0.711
	10 wt%	2.60	39 268	91.2	106.8	25.8/24.1/16.4	33.1	516	0.171, 0.721
	20 wt%	2.47	36 141	80.0	95.0	22.4/21.6/15.5	33.0	517	0.174, 0.722
	30 wt%	2.44	32 504	72.6	85.8	20.3/20.0/14.6	32.9	517	0.176, 0.723

[a] Turn-on voltage at a luminance of 1 cd m^{-2}. [b] Maximum luminance. [c] Maximum luminous efficiency. [d] Maximum power efficiency. [e] External quantum efficiency at maximum and at luminances of 100/1000 cd m^{-2}. [f] Full-width at half-maximum at 1000 cd m^{-2}. [g] EL maximum at 1000 cd m^{-2}. [h] CIE coordinates at 1000 cd m^{-2}.

seen that the maximum EQEs are obtained at doping concentrations of 1 wt% and 3 wt%, which are 25.2% and 26.5% for **BThPAc-1** and **BThPAc-2**, respectively, much higher than that of **PAc** ($EQE_{max} = 20.7\%$) at the same doping concentration. At the practical luminance of 100 cd A^{-1}, EQEs for **BThPAc-1** and **BThPAc-2** are maintained at 20.6% and 22.0%, respectively. The maximum luminous efficiencies (LEs) are 87.9 and 91.2 cd A^{-1} for **BThPAc-1** and **BThPAc-2**, respectively, corresponding to maximum power efficiencies (PEs) of 98.7 and 106.8 Im W^{-1}, respectively, which are about two-fold that of **PAc** (48.5 Im W^{-1}). Importantly, **BThPAc-1** and **BThPAc-2** still exhibit high efficiency at a high doping concentration of 30 wt%, with the maximum EQE/LE/PE of 17.0%/62.7 cd A^{-1}/75.5 Im W^{-1} for **BThPAc-1** and 20.3%/72.6 cd A^{-1}/85.8 Im W^{-1} for **BThPAc-2**. These results suggest that the **DBDPA**-based MR-TADF emitters can be an effective approach to realize high device efficiency for green emission with CIE $y > 0.7$ even at relatively high doping concentrations (>15 wt%).

3 Conclusions

In summary, we have developed two multiple resonance emitters (**BThPAc-1** and **BThPAc-2**) containing a 10-dibenzothiophenyl-9,9-diphenylacridane-based B, N-doped polycyclic aromatic skeleton for efficient narrowband green emission at high doping concentrations. The two carbon-bridged phenyl rings of the dibenzothiophenyl-9,9-diphenylacridane segment provide steric hindrance to suppress the aggregation of the polycyclic skeleton, while the dibenzothiophene moiety could extend the conjugation to red-shift the emission to the green region. As a result, **BThPAc-1** and **BThPAc-2** exhibit green emissions of 509–510 nm with a narrow FWHM of 32 nm at 1 wt% doping concentration, which are maintained at 515–520 nm with narrow FWHMs of 34–35 nm as the doping concentration increases to 100 wt%. Meanwhile, the sulfur atom can enhance spin–orbital coupling by the heavy-atom effect, leading to the accelerated RISC process with a rate constant of 1.1–1.2 $\times$ 10^5 s^{-1}. OLED devices based on the emitters exhibit green emission with an emission peak at 514 nm, an FWHM of 33 nm and a maximum EQE of 26.5% at 3 wt% doping concentration. Importantly, the OLED devices still maintain the small FWHM of 33 nm and CIE coordinates of (0.18, 0.72), together with a high maximum EQE of 20.3% even at a doping concentration of 30 wt%, which is remarkable for green MR-TADF emitters with CIE $y > 0.7$ at high doping concentrations. These findings provide a facile and effective molecular design strategy for the development of aggregation-resistant multi-resonance emitters to realize efficient narrowband green emissions in wide doping concentration ranges.

Data availability

The data supporting this article have been included as part of the ESI.†

Author contributions

Rui Zhong synthesized the emitters and characterized the photophysical property. Mengyu Wang and Shumeng Wang fabricated and characterized the OLED devices. Xingdong Wang and Shiyang Shao provided guidance on synthesis and photophysical characterization. Rui Zhong and Shiyang Shao wrote the manuscript. L. W. supervised and directed this study.

Conflicts of interest

There are no conflicts to declare.

Acknowledgements

The authors acknowledge financial support from the National Natural Science Foundation of China (52122309, 52073282, 21975247, and 52261135541), the CAS-Croucher Funding Scheme for Joint Laboratories, the Innovational Fund for Scientific and Technological Personnel of Hainan Province (KJRC2023C09), the Open Project of State Key Laboratory of Supramolecular Structure and Materials (sklssm2024024), Start-up Scientific Research Foundation from Hainan University (KYQD(ZR)22174). The authors also acknowledge the staff of the BL17B beamline of National Facility for Protein Science in Shanghai (NFPS) at the Shanghai Synchrotron Radiation Facility for assistance in crystal structure data collection and the Network and Computing Center, Changchun Institute of Applied Chemistry, Chinese Academy of Sciences for help with theoretical calculations.

References

1 A. Endo, K. Sato, K. Yoshimura, T. Kai, A. Kawada, H. Miyazaki and C. Adachi, *Appl. Phys. Lett.*, 2011, **98**, 083302.
2 R. K. Konidena and J. Y. Lee, *Chem. Rec.*, 2019, **19**, 1499.
3 H. Uoyama, K. Goushi, K. Shizu, H. Nomura and C. Adachi, *Nature*, 2012, **492**, 234.
4 Z. Yang, Z. Mao, Z. Xie, Y. Zhang, S. Liu, J. Zhao, J. Xu, Z. Chi and M. P. Aldred, *Chem. Soc. Rev.*, 2017, **46**, 915.
5 L.-S. Cui, A. J. Gillett, S.-F. Zhang, H. Ye, Y. Liu, X.-K. Chen, Z.-S. Lin, E. W. Evans, W. K. Myers, T. K. Ronson, H. Nakanotani, S. Reineke, J.-L. Bredas, C. Adachi and R. H. Friend, *Nat. Photonics*, 2020, **14**, 636.
6 Y. Liu, C. Li, Z. Ren, S. Yan and M. R. Bryce, *Nat. Rev. Mater.*, 2018, **3**, 18020.
7 W. Yuan, H. Yang, C. Duan, X. Cao, J. Zhang, H. Xu, N. Sun, Y. Tao and W. Huang, *Chem*, 2020, **6**, 1998.
8 Y. Im, M. Kim, Y. J. Cho, J.-A. Seo, K. S. Yook and J. Y. Lee, *Chem. Mater.*, 2017, **29**, 1946.
9 F. Santoro, A. Lami, R. Improta, J. Bloino and V. Barone, *J. Chem. Phys.*, 2008, **128**, 224311.
10 M. Y. Wong and E. Zysman-Colman, *Adv. Mater.*, 2017, **29**, 1605444.
11 T. Hatakeyama, K. Shiren, K. Nakajima, S. Nomura, S. Nakatsuka, K. Kinoshita, J. Ni, Y. Ono and T. Ikuta, *Adv. Mater.*, 2016, **28**, 2777.

12 H. J. Kim and T. Yasuda, *Adv. Opt. Mater.*, 2022, **10**, 2201714.
13 S. Madayanad Suresh, D. Hall, D. Beljonne, Y. Olivier and E. Zysman-Colman, *Adv. Funct. Mater.*, 2020, **30**, 1908677.
14 K. R. Naveen, P. Palanisamy, M. Y. Chae and J. H. Kwon, *Chem. Commun.*, 2023, **59**, 3685.
15 S. Oda, B. Kawakami, R. Kawasumi, R. Okita and T. Hatakeyama, *Org. Lett.*, 2019, **21**, 9311.
16 F. Chen, L. Zhao, X. Wang, Q. Yang, W. Li, H. Tian, S. Shao, L. Wang, X. Jing and F. Wang, *Sci. China: Chem.*, 2021, **64**, 547.
17 D. Hall, S. M. Suresh, P. L. dos Santos, E. Duda, S. Bagnich, A. Pershin, P. Rajamalli, D. B. Cordes, A. M. Z. Slawin, D. Beljonne, A. Köhler, I. D. W. Samuel, Y. Olivier and E. Zysman-Colman, *Adv. Opt. Mater.*, 2019, **8**, 1901627.
18 T. Hua, L. Zhan, N. Li, Z. Huang, X. Cao, Z. Xiao, S. Gong, C. Zhou, C. Zhong and C. Yang, *Chem. Eng. J.*, 2021, **426**, 131169.
19 Q. Li, Y. Wu, X. Wang, Q. Yang, J. Hu, R. Zhong, S. Shao and L. Wang, *Chem.–Eur. J.*, 2022, **28**, e202104214.
20 Q. Li, Y. Wu, Q. Yang, S. Wang, S. Shao and L. Wang, *ACS Appl. Mater. Interfaces*, 2022, **14**, 49995.
21 H. Min, I. S. Park and T. Yasuda, *Angew. Chem., Int. Ed.*, 2021, **60**, 7643.
22 M. Nagata, H. Min, E. Watanabe, H. Fukumoto, Y. Mizuhata, N. Tokitoh, T. Agou and T. Yasuda, *Angew. Chem., Int. Ed.*, 2021, **60**, 20280.
23 W. Ning, H. Wang, S. Gong, C. Zhong and C. Yang, *Sci. China: Chem.*, 2022, **65**, 1715.
24 I. S. Park, H. Min and T. Yasuda, *Angew. Chem., Int. Ed.*, 2022, **61**, e202205684.
25 I. S. Park, M. Yang, H. Shibata, N. Amanokura and T. Yasuda, *Adv. Mater.*, 2022, **34**, 2107951.
26 X. Wu, J. W. Huang, B. K. Su, S. Wang, L. Yuan, W. Q. Zheng, H. Zhang, Y. X. Zheng, W. Zhu and P. T. Chou, *Adv. Mater.*, 2022, **34**, 2105080.
27 Y. Yuan, X. Tang, X. Y. Du, Y. Hu, Y. J. Yu, Z. Q. Jiang, L. S. Liao and S. T. Lee, *Adv. Opt. Mater.*, 2019, **7**, 1801536.
28 S. Oda, B. Kawakami, Y. Yamasaki, R. Matsumoto, M. Yoshioka, D. Fukushima, S. Nakatsuka and T. Hatakeyama, *J. Am. Chem. Soc.*, 2022, **144**, 106.
29 S. Oda, T. Sugitani, H. Tanaka, K. Tabata, R. Kawasumi and T. Hatakeyama, *Adv. Mater.*, 2022, **34**, 2201778.
30 Y. Xu, Z. Cheng, Z. Li, B. Liang, J. Wang, J. Wei, Z. Zhang and Y. Wang, *Adv. Opt. Mater.*, 2020, **8**, 1902142.
31 M. Yang, I. S. Park and T. Yasuda, *J. Am. Chem. Soc.*, 2020, **142**, 19468.
32 M. Yang, S. Shikita, H. Min, I. S. Park, H. Shibata, N. Amanokura and T. Yasuda, *Angew. Chem., Int. Ed.*, 2021, **60**, 23142.
33 Y. Zhang, D. Zhang, T. Huang, A. J. Gillett, Y. Liu, D. Hu, L. Cui, Z. Bin, G. Li, J. Wei and L. Duan, *Angew. Chem., Int. Ed.*, 2021, **60**, 20498.
34 Y. C. Cheng, X. C. Fan, F. Huang, X. Xiong, J. Yu, K. Wang, C. S. Lee and X. H. Zhang, *Angew. Chem., Int. Ed.*, 2022, **61**, e202212575.
35 Y. X. Hu, J. Miao, T. Hua, Z. Huang, Y. Qi, Y. Zou, Y. Qiu, H. Xia, H. Liu, X. Cao and C. Yang, *Nat. Photonics*, 2022, **16**, 803.
36 Y. Kondo, K. Yoshiura, S. Kitera, H. Nishi, S. Oda, H. Gotoh, Y. Sasada, M. Yanai and T. Hatakeyama, *Nat. Photonics*, 2019, **13**, 678.
37 Q. Wang, Y. Xu, T. Yang, J. Xue and Y. Wang, *Adv. Mater.*, 2023, **35**, 2205166.
38 Y. Zhang, J. Wei, L. Wang, T. Huang, G. Meng, X. Wang, X. Zeng, M. Du, T. Fan, C. Yin, D. Zhang and L. Duan, *Adv. Mater.*, 2023, **35**, 2209396.
39 Y. Zou, J. Hu, M. Yu, J. Miao, Z. Xie, Y. Qiu, X. Cao and C. Yang, *Adv. Mater.*, 2022, **34**, 2201442.
40 S. Cai, G. S. M. Tong, L. Du, G. K. So, F. F. Hung, T. L. Lam, G. Cheng, H. Xiao, X. Chang, Z. X. Xu and C. M. Che, *Angew. Chem., Int. Ed.*, 2022, **61**, e202213392.
41 X. Fan, X. Hao, F. Huang, J. Yu, K. Wang and X. Zhang, *Adv. Sci.*, 2023, **10**, 2303504.
42 X.-C. Fan, K. Wang, Y.-Z. Shi, Y.-C. Cheng, Y.-T. Lee, J. Yu, X.-K. Chen, C. Adachi and X.-H. Zhang, *Nat. Photonics*, 2023, **17**, 280.
43 Y. Hu, J. Miao, C. Zhong, Y. Zeng, S. Gong, X. Cao, X. Zhou, Y. Gu and C. Yang, *Angew. Chem., Int. Ed.*, 2023, **62**, e202302478.
44 J. Liu, Y. Zhu, T. Tsuboi, C. Deng, W. Lou, D. Wang, T. Liu and Q. Zhang, *Nat. Commun.*, 2022, **13**, 4876.
45 Y. Liu, X. Xiao, Z. Huang, D. Yang, D. Ma, J. Liu, B. Lei, Z. Bin and J. You, *Angew. Chem., Int. Ed.*, 2022, **61**, e202210210.
46 X. F. Luo, S. Q. Song, H. X. Ni, H. Ma, D. Yang, D. Ma, Y. X. Zheng and J. L. Zuo, *Angew. Chem., Int. Ed.*, 2022, **61**, e202209984.
47 S. Uemura, S. Oda, M. Hayakawa, R. Kawasumi, N. Ikeda, Y. T. Lee, C. Y. Chan, Y. Tsuchiya, C. Adachi and T. Hatakeyama, *J. Am. Chem. Soc.*, 2023, **145**, 1505.
48 J. Wang, N. Li, C. Zhong, J. Miao, Z. Huang, M. Yu, Y. X. Hu, S. Luo, Y. Zou, K. Li and C. Yang, *Adv. Mater.*, 2023, **35**, 2208378.
49 M. Wang, Z. Fu, R. Cheng, J. Du, T. Wu, Z. Bin, D. Wu, Y. Yang and J. Lan, *Chem. Commun.*, 2023, **59**, 5126.
50 Q. Wang, Y. Xu, T. Huang, Y. Qu, J. Xue, B. Liang and Y. Wang, *Angew. Chem., Int. Ed.*, 2023, **62**, e202301930.
51 Y. Zhang, G. Li, L. Wang, T. Huang, J. Wei, G. Meng, X. Wang, X. Zeng, D. Zhang and L. Duan, *Angew. Chem., Int. Ed.*, 2022, **61**, e202202380.
52 G. Chen, J. Wang, W. C. Chen, Y. Gong, N. Zhuang, H. Liang, L. Xing, Y. Liu, S. Ji, H. L. Zhang, Z. Zhao, Y. Huo and B. Z. Tang, *Adv. Funct. Mater.*, 2023, **33**, 2211893.
53 B. Du, K. Zhang, P. Wang, X. Wang, S. Wang, S. Shao and L. Wang, *J. Mater. Chem. C*, 2023, **11**, 9578.
54 T. Fan, Y. Zhang, L. Wang, Q. Wang, C. Yin, M. Du, X. Jia, G. Li and L. Duan, *Angew. Chem., Int. Ed.*, 2022, **61**, e202213585.
55 L. Liang, C. Qu, X. Fan, K. Ye, Y. Zhang, Z. Zhang, L. Duan and Y. Wang, *Angew. Chem., Int. Ed.*, 2024, **63**, e202316710.
56 F. Liu, Z. Cheng, L. Wan, Z. Feng, H. Liu, H. Jin, L. Gao, P. Lu and W. Yang, *Small*, 2022, **18**, 2106462.

57 J. Park, K. J. Kim, J. Lim, T. Kim and J. Y. Lee, *Adv. Mater.*, 2022, **34**, 2108581.
58 Y. K. Qu, D. Y. Zhou, F. C. Kong, Q. Zheng, X. Tang, Y. H. Zhu, C. C. Huang, Z. Q. Feng, J. Fan, C. Adachi, L. S. Liao and Z. Q. Jiang, *Angew. Chem., Int. Ed.*, 2022, **61**, e202201886.
59 L. Xiaofeng, Z. Dongdong, D. Lian and Z. Yuewei, *Front. Chem.*, 2023, **11**, 1198404.
60 J. Bian, S. Chen, L. Qiu, R. Tian, Y. Man, Y. Wang, S. Chen, J. Zhang, C. Duan, C. Han and H. Xu, *Adv. Mater.*, 2022, **34**, 2110547.
61 Y. Chang, Y. Wu, K. Zhang, S. Wang, X. Wang, S. Shao and L. Wang, *Dyes Pigm.*, 2023, **220**, 111678.
62 H. J. Cheon, S. J. Woo, S. H. Baek, J. H. Lee and Y. H. Kim, *Adv. Mater.*, 2022, **34**, 2207416.
63 Y. N. Hu, X. C. Fan, F. Huang, Y. Z. Shi, H. Wang, Y. C. Cheng, M. Y. Chen, K. Wang, J. Yu and X. H. Zhang, *Adv. Opt. Mater.*, 2022, **11**, 2202267.
64 F. Huang, X. C. Fan, Y. C. Cheng, H. Wu, Y. Z. Shi, J. Yu, K. Wang, C. S. Lee and X. H. Zhang, *Mater. Horiz.*, 2022, **9**, 2226.
65 P. Jiang, J. Miao, X. Cao, H. Xia, K. Pan, T. Hua, X. Lv, Z. Huang, Y. Zou and C. Yang, *Adv. Mater.*, 2022, **34**, 2106954.
66 X. F. Luo, H. X. Ni, X. Liang, D. Yang, D. Ma, Y. X. Zheng and J. L. Zuo, *Adv. Opt. Mater.*, 2023, **11**, 2203002.
67 Y. Xu, C. Li, Z. Li, Q. Wang, X. Cai, J. Wei and Y. Wang, *Angew. Chem., Int. Ed.*, 2020, **59**, 17442.
68 Y. Zhang, J. Wei, D. Zhang, C. Yin, G. Li, Z. Liu, X. Jia, J. Qiao and L. Duan, *Angew. Chem., Int. Ed.*, 2022, **61**, e202113206.
69 N. Peethani, N. Y. Kwon, C. W. Koh, S. H. Park, J. M. Ha, M. J. Cho, H. Y. Woo, S. Park and D. H. Choi, *Adv. Opt. Mater.*, 2023, **12**, 2301217.
70 A. Pershin, D. Hall, V. Lemaur, J. C. Sancho-Garcia, L. Muccioli, E. Zysman-Colman, D. Beljonne and Y. Olivier, *Nat. Commun.*, 2019, **10**, 597.